University of Seville

Degree in Physics

Magnetic Diagnostics for the SMall Aspect Ratio Tokamak of the University of Seville

Fernando Puentes del Pozo

Supervisores:

Manuel García Muñoz

Alessio Mancini

Diego Cruz Zabala

Departamento de Física Atómica, Molecular y Nuclear

Facultad de Física

Agradecimientos

Me gustaría agradecer al grupo de PSFT por la oportunidad de realizar este trabajo y por toda la ayuda que me han prestado para desarrollarlo, en especial a Diego Cruz y Alessio Mancini que me han guiado y ayudado durante todo el proceso.

También me gustaría agradecer a mis compañeros y amigos por todo el apoyo y los buenos momentos que hemos pasado estos años.

Finalmente me gustaría agradecer a mi familia, a mi madre que me inculcó su serenidad, a mi padre que me inculcó su amor por la física, y a mi hermana María a la que me gustaría dedicar este trabajo.

Resumen

El SMall Aspect Ratio Tokamak es un tokamak esférico que se encuentra en proceso de construcción en la Universidad de Sevilla. Varios sistemas de diagnóstico magnético basados en sensores inductivos han sido diseñados para su instalación en este tokamak.

Entre ellos se incluye un conjunto de bobinas de Rogowski empleadas para medir la corriente del plasma y las corrientes de Eddy en las paredes de la cámara de vacío. También se incluye un conjunto de bobinas de Mirnov utilizadas para la reconstrucción del equilibrio del plasma y otro conjunto para la detección de modos inestables de hasta 200kHz de frecuencia.

Estos diagnósticos son descritos en detalle y tambien lo son las consideraciones tenidas en cuenta para su diseño así como una propuesta para su calibración.

Abstract

The SMall Aspect Ratio Tokamak is a spherical tokamak that is in building process in the University of Seville. Various magnetic diagnostic systems based on inductive sensors have been designed for their installation in this tokamak.

Among them there is a set of Rogowski coils that are employed to measure the plasma current and the Eddy currents in the walls of the vacuum chamber. Moreover there is also an array of Mirnov coils used for the plasma equilibrium reconstruction and another set for the detection of unstable modes of up to 200kHz of frequency.

These diagnostics are described in detail and so are the considerations taken into account for their design along with a proposal for their calibration.

Contents

Chapter 1

Motivation

1.1 Nuclear fusion.

The modern human lifestyle is completely dependant on energy, there is a direct correlation between the quality of life in a region and it's energy consumption per capita [1]. As society and technology continues to develop, the energy demand of the world will continue to increase and we will need to find a way to satisfy it.

As of today, most energy production comes from fossil fuels (Fig. 1.1) which are non renewable and very contaminating. In order to maintain the world energy supply over the next century it will be imperative to find other alternatives. Renewable energy sources, such as solar or eolic, are very promising, but they are not energy dense enough to provide energy to big cities. Nuclear fission in the other hand is very energy dense but it produces very long lasting nuclear waste and has a bad public opinion due to safety concerns.

Nuclear fusion stands out as the long term solution to the worlds energy crisis. It is extremely energy dense, the radioactive products are short lived and it does not produce greenhouse emissions. On top of that, the necessary fuel is virtually endless and easy to access for any country, which would put an end to the fuel related political conflicts. As we can see, the development of the scientific and technological advances necessary for widespread use of nuclear fusion for energy production would be extremely beneficial.

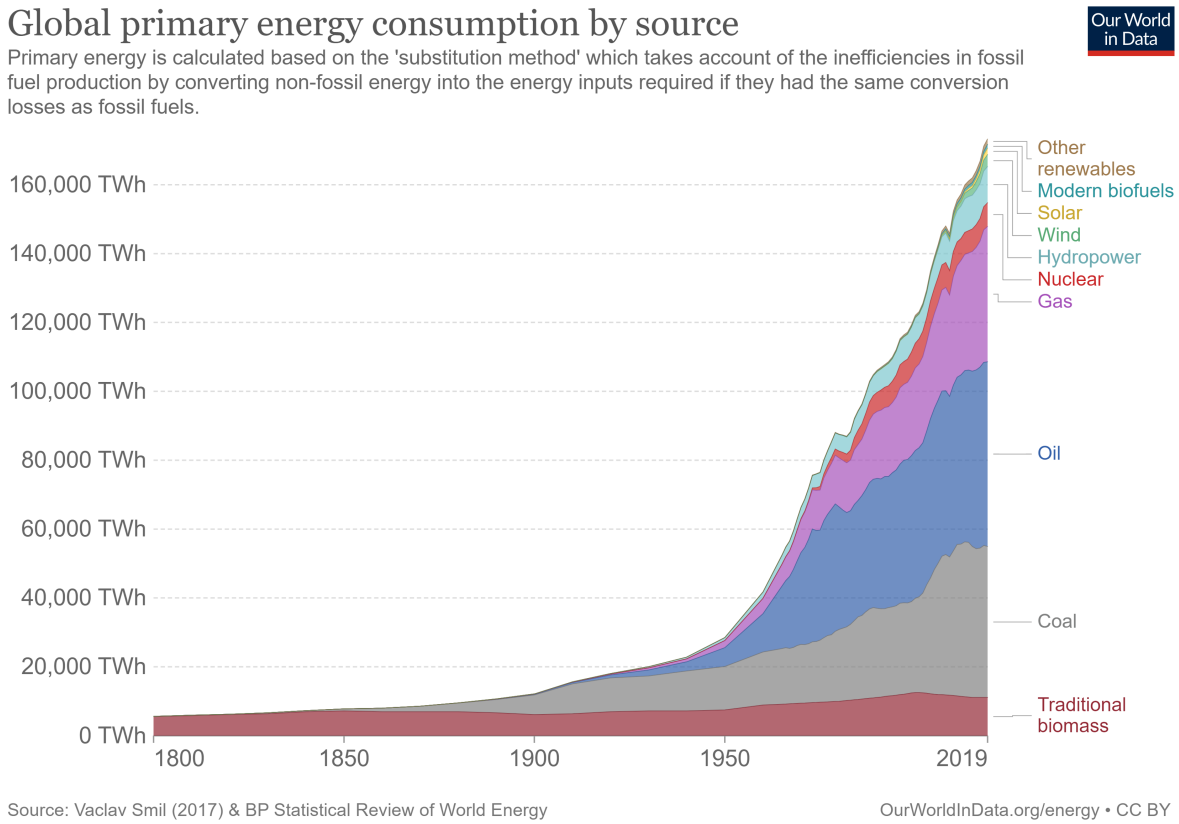

Figure 1.1: Global energy consumption by source in the last centuries.

Chapter 2

Theoretical introduction

2.1 Thermonuclear fusion

Nuclear fusion is the process through which two light nuclei fuse to create a heavier one, emitting a great amount of energy due to the mass difference between the initial and final particles. This process takes place in stars like the sun and is the source of their energy. The most common example of fusion is the reaction between deuterium and tritium to form helium

$$D + T \rightarrow {}^4He + n + 17.6MeV \tag{2.1}$$

For this reaction to take place, first we need to overcome the repulsive electrostatic force between the two nuclei so that we can bring them close enough for the strong nuclear force to bind them together [2]. Quantum tunneling will help the nuclei fuse, but we will still need to provide some energy. In thermonuclear fusion we provide this energy thermally, for the reaction to occur we will need a temperature in the order of $\sim$ 10 keV or $\sim$ 100 million K.

On top of heating up the fuel to this temperatures, which will transform it into a plasma, we also need enough density and to hold the particles together for long enough so that the reaction can take place. In the meantime we need to make sure that it does not make contact with any material medium as it would cool the fuel. Therefore we need to create a high vacuum and to confine the the plasma. There are two main approaches to this confinement [2].

In inertial confinement fusion, the fuel is stored in small pellets and is then heated up externally and detonated by powerful lasers or particle beams. The fuel is rapidly consumed and is confined by it's own inertia [2].

2.2 Magnetic confinement. The tokamak.

In magnetic confinement fusion, the fuel plasma is confined by strong magnetic fields that create magnetic bottles trapping the plasma particles. Charged particles in a plasma will follow magnetic field lines due to the Lorentz force $\vec{F} = q \cdot \vec{v} \wedge \vec{B}$. In this way we could, on first approximation, keep the particles confined for an arbitrary time period so that we can produce fusion.

One of the most widespread designs for this kind of device is the tokamak Fig. 2.1. In a tokamak the plasma is confined in a toroidal shape by a toroidaly symmetric helicoidal magnetic field created by a system of coils and the own plasma current[3].

The toroidal magnetic field, B_ϕ, is created by a set of toroidal field coils (TFC) each of which surround the torus in the poloidal direction. The poloidal magnetic field, B_p, is created by the plasma current, I_p, which is induced by a large central solenoid (CS) in the center of the torus that couples with the plasma like a electrical transformer would.

Finally, the plasma under this field configuration suffer a so called "hoop force", that tries to expand the plasma torus radially outwards. To prevent this we need a vertical magnetic field that is created by a set of horizontal coils called poloidal field coils (PFC) [2].

2.3 Plasma.

Author in [4] defines plasma as "*a quasineutral gas of charged and neutral particles which exhibits collective behavior*". Collective behavior, in contrast with the individual behavior presented by a typical gas where particles interact with each other in short range, two particle collisions; means that particles in a plasma can interact through long range electromagnetic forces.

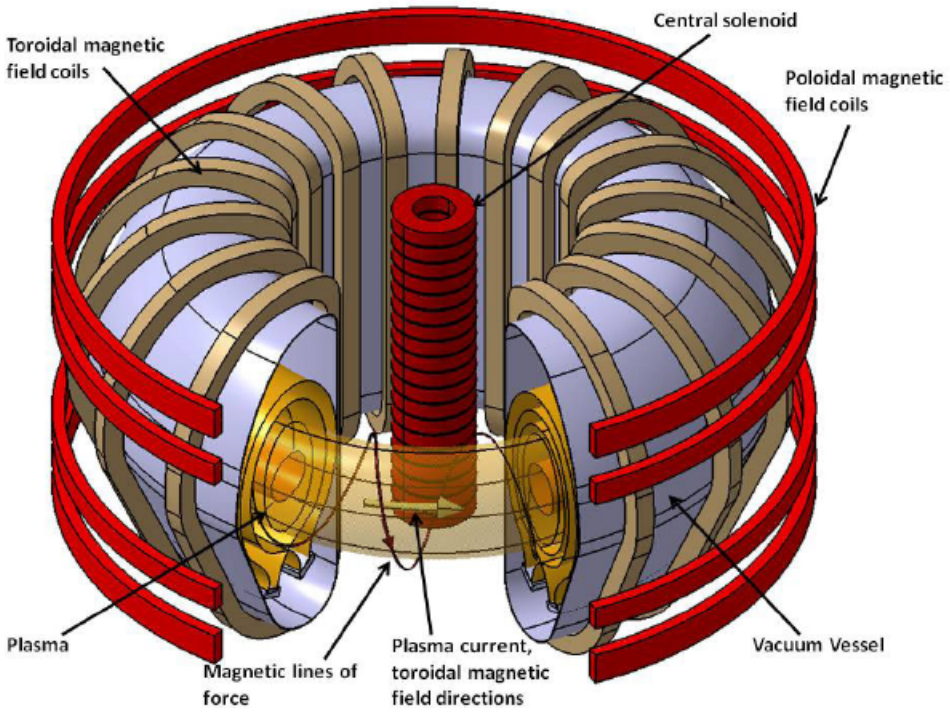

Figure 2.1: Schematic of the coils and fields in a tokamak [2].

In a plasma, the charged particles can move to create local concentrations of positive or negative charge that can interact with other charge concentrations through Coulomb force. This collective behavior implies that the movement of the particles of the plasma does not depend only on local conditions, but also on the global state of the plasma.

To explain the quasineutrality property we will look into the Debye shielding effect. If we introduce a positive charge distribution inside a plasma, the electric field created will attract the negative charge particles in the plasma and repel the positive ones. Gauss law for electrostatic fields then tells us that the field far away from the charge distribution will be screened by those negatively charged particles. Through Poisson's equation it can be shown [4] that the electrostatic potential, ϕ, will follow an exponential law of the form

$$\phi = \phi_0 e^{-r/\lambda_D} \quad ; \quad \lambda_D = \left(\frac{\varepsilon_0 K_B T_e}{n e^2}\right)^{1/2} \tag{2.2}$$

where K_B is Boltzmann's constant, T_e is the electron temperature, n is the plasma particle density and λ_D is the Debye length. With this effect in mind, quasineutrality means

that if the typical dimension of the plasma L is much grater than the Debye length, any local charge concentration or external electric field will be screened and the interior of the plasma will be free of any macroscopic fields.

To sum up, the are three conditions that a gas must satisfy in order to be classified as a plasma. We need enough particle density so that it makes sense to use a statistical description, we need a volume big enough so that the quasineutrality condition can be satisfied and we need collective interactions to dominate over two particle collisions. This conditions can be summarized in three physical relations.

Defining the plasma frequency, ω_P, as the frequency at which plasma particles can react to shield an external field, the mean time between two particle collisions, τ, and N_D as the number of particles in a Debye sphere, i.e.

$$N_D = n\frac{4}{3}\pi\lambda_D^3 \tag{2.3}$$

a plasma must verify the following conditions [4]:

$$\begin{aligned} &\lambda_D \ll L \\ &N_D \ggg 1 \\ &\omega\tau > 1 \end{aligned} \tag{2.4}$$

2.4 Plasma confinement.

The problem of plasma confinement can be divided into two, the plasma equilibrium and the plasma stability. The plasma must be in a stationary state and this state must not be disturbed. We will need both conditions in order to confine the plasma long enough for fusion to take place. Lets start by discussing the former.

2.4.1 MHD equilibrium and the G-S equation.

Magnetohidrodynamics (MHD) describes a plasma as fluid of charged particles and predicts it's behavior with a set of partial differential equations that combine Maxwell's and fluid equations. In order to describe an MHD equilibrium we will need to find a stationary solution to this equations [4].

As we have discussed, magnetic field lines inside a tokamak follow helicoidal paths advancing in the toroidal direction. This field configuration creates a series of nested toroidal magnetic surfaces that contain the magnetic field lines [3]. In an axisymmetrical equilibrium, the pressure and magnetic forces must cancel out. This relation can be described by the following equation

$$\vec{j} \wedge \vec{B} = \vec{\nabla} p \tag{2.5}$$

From this equation we know that pressure is constant along a magnetic field line and that current lines will also be contained inside the field surfaces, forming and angle with the field lines. We can define the plasma β as the ratio of the plasma pressure and the magnetic pressure, i.e.

$$\beta = \frac{p}{p_{mag}} = \frac{p}{B^2/2\mu_0} \tag{2.6}$$

The plasma β will change depending on the configuration of the fields and the plasma, and will indicate how efficiently we can confine the plasma [4]. The higher the β of the plasma, the less intense the necessary fields will be to confine a plasma of a given pressure.

A magnetic field with axial symmetry can be described by a scalar function. In the case of toroidal symmetry we can use the poloidal magnetic flux, ψ, i.e. the flux of poloidal magnetic field in a horizontal circle that extends to a given point in the poloidal plane, as such function [2]. This poloidal flux will be constant inside a toroidal field surface [3]

$$\vec{B} \cdot \vec{\nabla} \psi = 0 \tag{2.7}$$

An equivalent flux function can be defined for current lines, f, and it will have similar properties. As both functions depend of the plasma pressure, one can be expressed in terms of the other [3].

Taking into account that the solution is axisymmetric and therefore will not depend on the toroidal coordinate, and the relationships imposed by Maxwell's equations for stationary solutions

$$\begin{aligned} \vec{\nabla} \cdot \vec{B} &= 0 \\ \vec{\nabla} \wedge \vec{B} &= \mu_0 \vec{j} \end{aligned} \tag{2.8}$$

and substituting in equation (2.5), we can obtain the Grad-Shafranov equation (G-S equation) [3]

$$R\frac{\partial}{\partial R}\left(\frac{1}{R}\frac{\partial \psi}{\partial R}\right)+\frac{\partial^2 \psi}{\partial z^2}=-\mu_0 R^2 p'(\psi)-\mu_0^2 f(\psi)f'(\psi) \tag{2.9}$$

The G-S equation is a non linear partial differential equation that cannot be solved analytically but we can find numerical solutions that directly describe the plasma equilibrium and it's properties.

To solve the G-S we will need a set of boundary conditions for ψ that we can obtain with magnetic probes or poloidal flux coils placed at the surface of the plasma. Realistically, we cannot measure directly at the surface of the plasma as the measuring equipment would be damaged. But, with a set of measurements taken close enough to the plasma, we can extrapolate the field and obtain enough information to reconstruct the equilibrium [5].

In configurations with enough spacial symmetry, such as inside of a tokamak, we can simplify the problem slightly using space Fourier analysis. Using toroidal coordinates and supposing toroidal symmetry, the field can be decomposed in it's Fourier harmonics in the poloidal direction [5]:

$$B(\theta)=\frac{C_0}{2}+\sum_{m=1}^{\infty} C_m\cos(m\theta)+S_m\sin(m\theta) \tag{2.10}$$

where C_m and S_m are the Fourier decomposition coefficients and θ is the poloidal coordinate. This way of expressing the magnetic fields will allow us to obtain information about the structure of the magnetic fields and surfaces in a more intuitive manner.

The $m=0$ component will give us information about the diamagnetism of the plasma, that combined with measurements of the plasma resistivity, will give us the energy confinement time of the plasma [5]. Other components will give us information about the poloidal shape of the plasma [2]. For example, the $m=1$ component will give us information about the vertical and horizontal position of the plasma, the $m=2$ about it's ellipticity or elongation, κ, and the $m=3$ about it's triangularity, δ.

In a real tokamak, the field will not be completely symmetrical in the toroidal direction as we have a finite amount of PFC and the field created by them will decrease as move away from their center. In a similar manner as we did for the poloidal direction, we can also describe the variation of the fields in the toroidal direction by a spacial Fourier decomposition:

$$B(\phi) = \frac{\tilde{C}_0}{2} + \sum_{n=1}^{\infty} \tilde{C}_n \cos(n\phi) + \tilde{S}_n \sin(n\phi) \tag{2.11}$$

where ϕ is the toroidal coordinate and $\tilde{C}_n$ and $\tilde{S}_n$ are the coefficients of the decomposition.

2.4.2 MHD instabilities

A plasma in an equilibrium configuration can be disturbed by series of MHD instabilities that, if not dealt with, will rapidly grow until they create a disruption. A disruption is an undesirable event where the plasma confinement fails allowing a rapid collapse of the plasma temperature and current. The rate of change of plasma current in a disruption can reach upwards of 100MA/s, which will induce strong Eddy currents in the vessel walls and exert on them forces in the order of $10^5 Nm^{-2}$ [3].

It is clear that the detection and control of this instabilities will be essential for the safe operation of a tokamak. MHD instabilities arise from current gradients in the plasma and from pressure gradients combined with adverse magnetic field curvature. They can be divided into ideal modes that would occur even if the plasma was perfectly conductive and resistive modes that occur due to the finite conductivity of the plasma [3].

Instabilities are introduced as perturbations on the equilibrium field configuration. They are described by an infinite spectrum of modes that decompose the total perturbation by a Fourier transform in the toroidal and poloidal directions, similarly as in the case of the equilibrium fields [6]. Therefore this modes will have the form

$$\delta B(\theta, \phi) = \sum_{n,m}^{\infty} C_{nm} e^{i(m\theta + n\phi)} \tag{2.12}$$

In order to describe the generation of this modes from an axisymmetric equilibrium field configuration let us define the safety factor, q, as the number of turns in the poloidal direction a field line makes in a toroidal rotation for a given field surface [2]. We can determine q from integrating the field line equation in a field surface arriving at the expression [3]

$$q = \frac{\Delta\phi}{2\pi} = \frac{1}{2\pi} \oint \frac{1}{R} \frac{B_\phi}{B_p} ds \tag{2.13}$$

where R is the major radius of the torus and B_ϕ and B_p are the toroidal and poloidal fields respectively. It is important to note that q is a parameter of each field surface and

therefore is a function of the transversal position.

MHD instabilities will appear from equilibrium through small deviations and will resonate at the surfaces of $q = m/n$, as they have the same periodicity as the field in that surface, growing in amplitude [3]. As they grow they will deform the equilibrium field configuration, changing it's topology, until they create magnetic islands. Magnetic islands are regions where the field surface has been deformed until it has split into two, see Fig. 2.2.

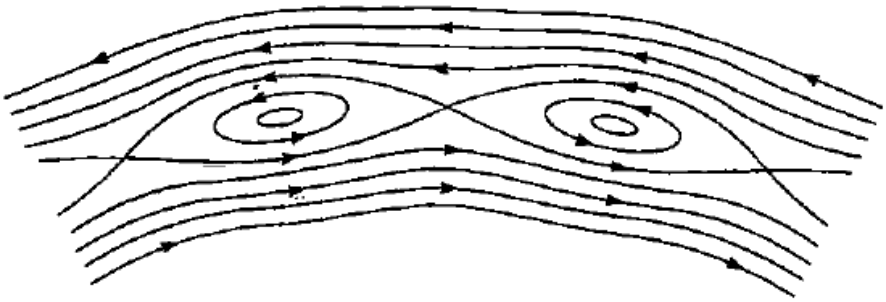

Figure 2.2: Creation of magnetic islands due to the deformations of the magnetic field [3]

The modes with lower m and n are usually dominant. $m = 1$ perturbations are commonly present, producing saw tooth shaped oscillations on the plasma density and temperature and on the magnetic fields outside of the plasma. This oscillations originate from magnetic islands that are formed at the $q = 1$ surface, where they grow until they replace the original field surface completely. The process then repeats itself as the perturbation travels toroidally, producing the denominated saw tooth instabilities [3].

Magnetic islands are created by the so called tearing modes in the region that surrounds the $q = m/n$ surfaces due to the finite conductivity of the plasma. This instabilities will grow the size of the magnetic islands exponentially until it saturates or a disruption takes place. If they are not dealt with, $m = 2$ modes can grow a magnetic island until it saturates in the order of 10ms [3].

Instabilities can also form in the current ramp-up phase. As the plasma current increases a negative current gradient forms at the plasma surface, at the same time, the poloidal field gradually increases, making the $q = m$ surfaces to expand outwards. When these surfaces reach the current gradient the respective mode gets excited creating tear-

ing modes denominated Mirnov instabilities with frequencies in the order of $1-10$kHz [3].

Finally, the MHD equations allow for the formation of waves inside the plasma denominated Alfvén waves. These waves will present an spectrum of eigenmodes that in the case of a tokamak, is a continuous spectrum [3]. This toroidal Alfvén modes (TAE) will create high frequency oscillations of the magnetic field in the range of 100kHz to several MHz.

Plasma instabilities will produce measurable perturbations in the magnetic fields outside of the plasma that we can measure with magnetic probes in order to detect them and control them before a disruption takes place [5].

2.5 Inductive sensors.

Inductive sensors are magnetic field measuring devices that are based in Faraday's law of induction.

$$V = -\frac{d\Phi_B}{dt} \tag{2.14}$$

Where V is the sensor's signal and Φ_B is the magnetic flux through the sensor. As such, they let us measure the time-derivative of magnetic fields or currents. This has two important implications. Firstly, we will only be capable of measuring non-constant fields or currents. Secondly, we will need to integrate the sensor's signal, either analogically or digitally to obtain the magnetic flux.

This kind of sensors were one of the first devices used for measuring magnetic fields and they still are widely spread nowadays, as they are simple, cheap and precise [7]. The simplest example of these sensors is a small coil of wire, supposing that the coil is small enough so that the magnetic field inside it can be considered approximately uniform, the voltage induced in the coil is [7]

$$V = -NA\frac{dB}{dt} = -\mu NA\frac{dH}{dt} \tag{2.15}$$

where N is the number of turns in the coil and A is it's area. If the field oscillates at a fixed frequency, f, or more generally, if we decompose an arbitrary field into it's Fourier frequency harmonics, the signal in the sensor will be

$$V = -\mu N A f H \tag{2.16}$$

In order to improve the sensitivity of the coil, i.e. the coefficient between the field to be measured and the sensor's signal, we can introduce a ferromagnetic core, so that equation (2.15) becomes

$$V = -\mu_0 \mu_r N A \frac{dH}{dt} \tag{2.17}$$

where μ_r is the relative magnetic permeability of the ferromagnetic core. This way we can greatly improve the sensor's sensitivity by up to two orders of magnitude. The price to pay for this increase in sensitivity will be the lost of linearity due to hysteresis effects in the ferromagnetic material.

From a circuitry view point, this kind of sensor will behave like an self inductance, L, in series with a resistance, R. We can estimate the self inductance and resistance of an air core coil of length, l, and diameter, D, made with a wire of resistivity, ρ, and diameter, d, as

$$L = N^2 \frac{\mu_0 A}{l} \tag{2.18}$$

$$R = \rho \frac{N D}{d^2/4} \tag{2.19}$$

At higher frequencies, we should also include in the model a parasitic capacitance connected in parallel to represent the capacitance created between the turns of conducting wire and other conductors [7], Fig. 2.3. This capacitance will depend strongly on how the coil is constructed and cannot be easily estimated beforehand.

Therefore, frequency ways these sensors will behave like a RLC circuit, that is, like a band pass filter Fig. (2.4). This circuit will have a resonance frequency given by [7]

$$f_c = \frac{1}{2\pi\sqrt{LC}} \tag{2.20}$$

At frequencies higher than f_c the output signal will start to drop. Adding a load resistance R_0 will be necessary in order to be able to measure the output signal and to improve the frequency response [7]. This load resistance will modify the frequency response curve that

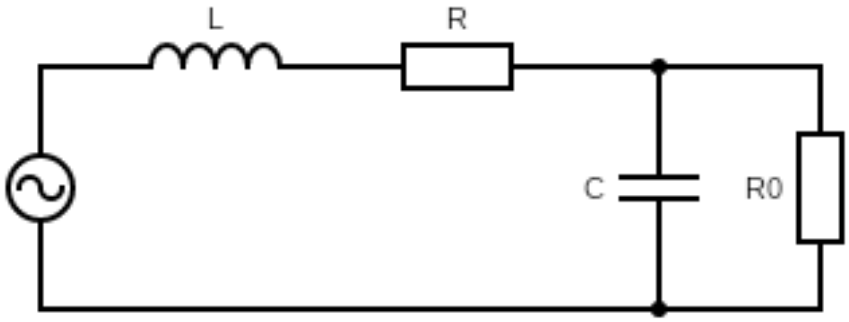

Figure 2.3: Circuit equivalent of an inductive sensor loaded with a resistance, R0

will now present a plateau in between two corner frequencies. The corner frequencies will depend on the coil parameters and the load resistance by [7]

$$\begin{aligned} f_l &= \frac{R + R_0}{2\pi L} \\ f_h &= \frac{1}{2\pi R_0 C} \end{aligned} \tag{2.21}$$

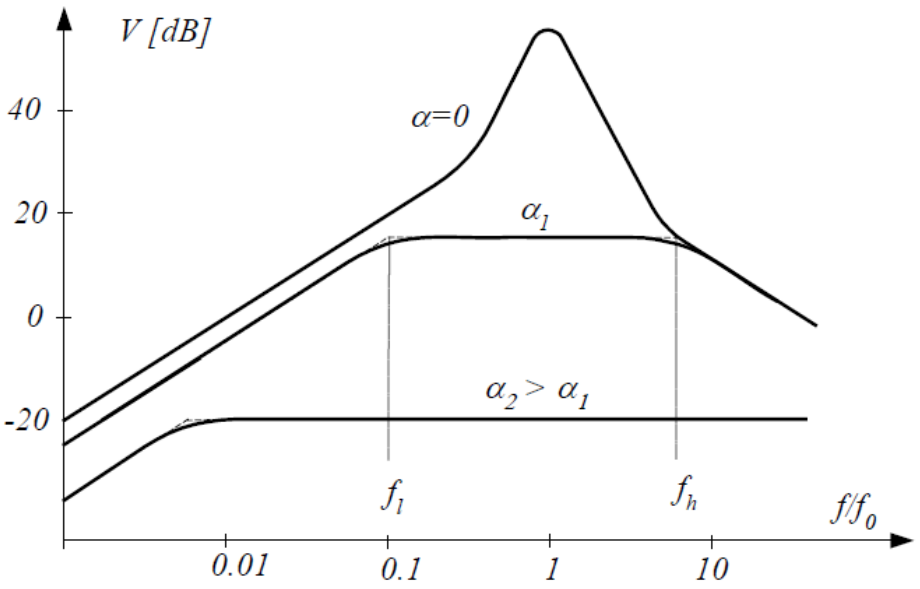

Figure 2.4: Frequency characteristics of an inductive sensor loaded with a resistance ($\alpha = R/R_0$) [7]

At lower frequencies, the signal will increase lineally with the frequency as predicted in equation (2.16), but at higher frequencies it will begin to drop. If the load resistance is

chosen so that $f_l > f_c$, the sensor's bandwidth will be only limited by f_c.

2.5.1 Rogowski coils.

Rogowski coils are inductive sensors used to measure currents, they are torus-shaped solenoids whose ends are brought together in order to link around the current to measure [5]. They are based on Ampere's law

$$\oint_l \vec{B} \cdot d\vec{l} = \mu I \tag{2.22}$$

where I is the total current enclosed in the closed path l, and μ is the magnetic permeability of the coil's core. Supposing the field to be almost constant inside of the coil, the total magnetic flux in the coil due to the field created by the encircled current can be described by

$$\Phi = nA\mu I \tag{2.23}$$

where n is the number of turns per unit length, so the coil signal can be finally expressed as

$$V = -\frac{d\Phi}{dt} = -nA\mu\frac{dI}{dt} \tag{2.24}$$

Magnetic flux through the solenoid's center would also create a electromotive force, there are two simple ways to prevent this. We can either use a return wire Fig. 2.5, or we can use an even number of windings in opposite directions.

Rogowski coils are highly versatile and can be used for a wide range of currents, from a few milliamperes to hundreds of kiloamperes, with a bandwidth that can reach several MHz [8]. They are completely non-intrusive as they do not need to be in contact with the current to measure, which is key in order to measure the plasma current.

On first approximation, the signal of a Rogowski coil is independent of the spacial distribution of the current inside it. In reality, if the current is not centered a small error will be caused. Still, Rogowski coils are not too sensible to this non-centrality effect and if the deviation is relatively small this error can be ignored [9].

The Rogowski coil working principle is strongly based on a good winding all around the loop of coil. Imperfections in this winding such as not uniform pitch advancement, turns

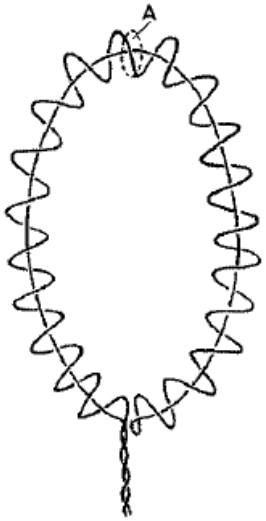

Figure 2.5: Schematic drawing of a Rogowski coil with a return wire [5].

not being exactly the same size or the discontinuity at the end of the coil where the coil's output is located, can add up to produce significant errors in the signal [10].

2.5.2 Mirnov coils

Mirnov coils, also commonly referred to as pick-up coils or magnetic probes, are wire coils that are mounted to the VC walls or other support structures, inside and outside of the VC, that are used to measure the magnetic fields in a tokamak [5]. Depending of how they are designed, they can serve multiple purposes.

Mirnov coils are used in the equilibrium field reconstruction for real time control of the plasma [5]. The poloidal and toroidal modes of the magnetic field described in equations (2.10) and (2.11) can be measured with an array of Mirnov coils. To do so, we will need one probe for the constant component, and two probe for each mode we wish to measure, one for the degree of freedom of the amplitude of the mode and one for the degree of freedom of the phase.

Each probe must measure, at least, the poloidal and the radial components of the field, the toroidal component can be assumed to be constant in an equilibrium configuration due to the symmetry of the problem and therefore does not need to be measured for the equilibrium reconstruction. To do so we will need at least two coils per probe oriented in perpendicular directions.

Mirnov coils can also be used to detect the formation of unstable modes in the plasma described in equation (2.12). As we have discussed, unstable modes will arise as perturbations to the equilibrium fields, and as such, they will have an amplitude orders of magnitude smaller. But they also have frequencies orders of magnitude greater than the equilibrium fields, note that sensor sensitivity will increase with frequency, as seen in equation (2.16). This will allow us the measure both the equilibrium fields and the instability fields with the same set of coils, as long as the cutoff frequency of the coils is greater than the frequency of the unstable mode [5].

In practice this will not be that simple. The coil's sensitivity increases linearly with the number of turns and the transversal section of the coil, at the same time, the resonance frequency of the coil decreases lineally with the number of turns and inversely to the square root of the transversal section, as can be seen in equations (2.16) and (2.20) [7].

$$\frac{V}{\dot{B}} \propto AN \qquad\qquad f_c \propto \frac{1}{N\sqrt{A}} \tag{2.25}$$

We can increase the bandwidth while keeping the same sensitivity by increasing the diameter of the coil and reducing the number of turns, but this approach is limited by the space constrains inside of the VC. Another approach would be to reduce the parasitic capacitance by increasing the spacing between turns of wire, but it runs into the same problem with the space constrains.

As a result, it is extremely hard to build a Mirnov coil that has enough sensitivity to measure the equilibrium fields while having enough bandwidth to detect the high frequency instabilities like the Alfvén modes ($\sim$ 100kHz) and while satisfying the space constrains.

A common solution for this problem is to use two different sets of coils, one for the equilibrium and low frequency instabilities (<1-20kHz) that can be designed to be more compact so that they can fit all around the plasma, and a smaller set of bigger coils with large bandwidth that can be installed in spots where more space is available [6, 11].

If we wish to measure M poloidal modes and N toroidal modes, in principle we will need $(2M+1)\times(2N+1)$ Mirnov coils distributed at regular intervals in the poloidal an toroidal directions. The number of coils needed can be greatly reduced if we can assume that only

one mode will be present at a given time, in which case we will only need one poloidal and one toroidal arrays, reducing the total number of coils to $(2M + 1) + (2N + 1)$ [6].

2.5.3 Poloidal flux loops.

Poloidal flux loops, or flux loops in short, are loops of wire that extend toroidally in the horizontal plane, measuring the poloidal magnetic flux, ψ, at a certain point in the poloidal plane. They are usually constructed with a single turn of wire and they are connected deferentially to a reference flux loop so as to cancel the poloidal flux created by the central solenoid, that would otherwise be the main contributor to the signal of the loop [12].

They are mainly used in the equilibrium reconstruction as they give us boundary conditions for the G-S equation, and therefore do not require a large bandwidth. They do not require calibration either, as their integrated signal is directly the poloidal flux. The unintegrated signal, with the proper correction to only remove the flux created by the CS, is the one-turn loop voltage [12], as the coil forms a 1-turn to 1-turn transformer with the plasma. The one-turn voltage combined with the measurement of the plasma current, I_p, made with a Rogowski coil, will allow us to determine the plasma conductivity.

The one-turn voltage of the plasma can reach several kV, so the wire used to built the loop must be able to withstand this high voltage.

2.5.4 Diamagnetic loops.

Diamagnetic loops are loops of wire that extend poloidally in a vertical plane, measuring the toroidal magnetic flux. They are called diamagnetic loops because they allow us to measure the diamagnetic properties of the plasma, which in turn have information about the plasma thermal energy [12] and the plasma selfinductance [5].

Diamagnetic loops not only measure the toroidal magnetic flux created by the diamagnetism of the plasma, they also measure the flux created by the TFC, which will be the main contributors to the loop's signal. To remove the undesired component of the magnetic flux, the diamagnetic loops have to be calibrated in the absence of plasma, and their signals compensated with the weighted signal of magnetic probes close to them and Rogowski coils installed around the power supply of the TFC.

In Fig. 2.6 we can see a schematic representation of the inductive sensors described in this section.

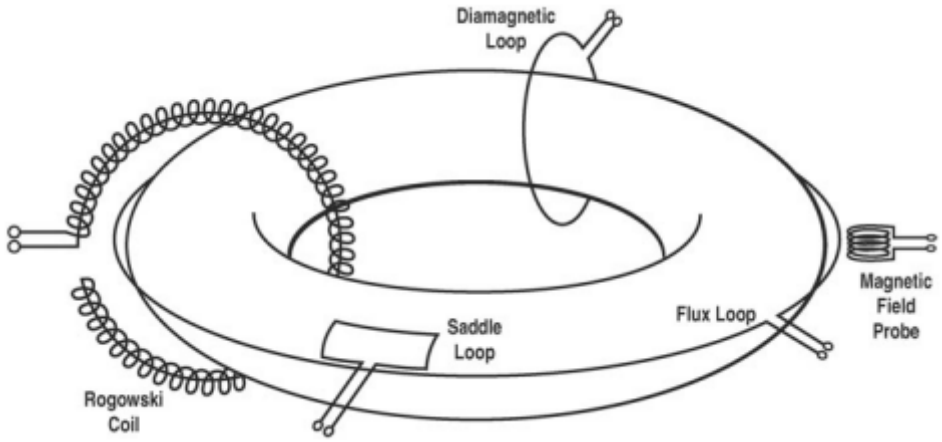

Figure 2.6: Schematic figure showing the inductive magnetic sensors commonly used in tokamaks, Rogowski coil, diamagnetic loop, magnetic probe, flux loop and saddle loop [12].

Chapter 3

Magnetic diagnostic design

Magnetic diagnostics have been designed for the SMART tokamak consisting of Rogowski and Mirnov coils, poloidal flux loops and diamagnetic loops. At the day of the publication of this work, it is yet to be constructed. Because of this, problems arising in the construction process and the final calibration of the system will not be discussed. Nevertheless, a proposal for calibration will be presented.

All signals extracted from the designed sensors will be digitized by an analog to digital converter with a -10V to 10V range. In some cases the signals will be processed analogically so the information obtained can be used in the real-time control of the plasma.

Materials chosen for the design of the diagnostics must be able to withstand radiation and temperatures of up to 500K, and and be suitable for high vacuum applications. This is the main reason why magnetic probes based on the Hall effect will not be used, as they are based in semiconductor technology and are therefore very sensible to temperature and radiation.

The maximum temperature that the diagnostics will have to withstand will occur during the ”baking” process, which is a process in which the VC is heated to around 500K in order to help extract the gases trapped inside the VC walls and other structures. This will ensure that a high vacuum can be created and that no contaminants will enter the plasma.

3.1 The SMART project.

Spherical tokamaks are magnetic confinement fusion devices with a low aspect ratio that are attractive because of how compact, cost effective and power dense they are when compared to conventional tokamaks. One of their important attributes is their high β coefficient, that as we have discussed, is the ratio between the plasma pressure and the magnetic pressure. This means that in order to obtain a certain plasma pressure the requirements for the confinement device will be lower [11, 13].

The SMall Sapect Ratio Tokamak (SMART) is a spherical tokamak being developed by the Plasma Science and Fusion Technology group of the University of Seville [14, 15, 16]. The objective of SMART is to serve as an educational fusion research device, to study plasma transport and confinement in both positive and negative triangularities, MHD stability control and the development of novel diagnostics in between others.

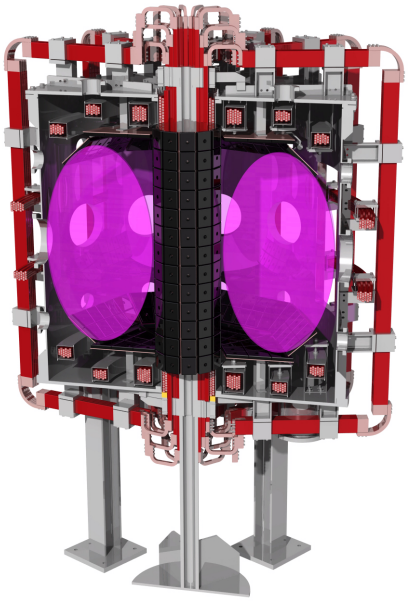

Figure 3.1: SMART cross section. Figure courtesy of the PSFT group.

The plasma in SMART is confined in a cylindrical vacuum chamber and surrounded by an assortment of coils used to confine the plasma Fig. 3.1 [14, 15]. The development of SMART is planned to have three phases of increasing plasma current, I_p, as the different systems are installed Table 3.1.

	Phase 1	**Phase 2**	**Phase 3**
Vessel radius (r_v) [m]	0.8		
Vessel height (h_v) [m]	1.6		
Plasma center (r_p) [m]	0.4		
Plasma radius (a) [m]	0.25		
Aspect ratio (A)	<2		
Plasma elongation (κ)	<2.1		
Plasma triangularity (δ)	±0.40	±0.50	±0.50
Toroidal field (B_ϕ) [T]	0.10	0.30	1.0
Plasma current (I_p) [kA]	30	100	500
Pulse length (τ) [ms]	20	100	500

Table 3.1: Physical parameters of SMART in the three phases of development [14, 16]

The plasma center radius, r_p, is the distance between the center of the tokamak's toroid and the center of the plasma's poloidal cross section. The plasma radius, a, is the distance between the center of the plasma and the plasma edge (Fig. 3.2). The aspect ratio, A, is the coefficient between the two. One of the objectives of the spherical tokamak design of the SMART is to reduce the aspect ratio bellow what we would find in a conventional toroidal tokamak, making it more compact and efficient.

The plasma elongation, κ, and triangularity, δ, describe the shape of the poloidal cross section of the plasma profile. The VC and coil system in SMART have been designed in order to support a wide range of plasma shapes so as to allow the study of it's effect on confinement time, edge stability and electron heat transport [14, 15, 16].

The biggest change in between phases will be the toroidal field created by the PFC, the plasma current and the pulse length. As new systems are constructed and installed, such as the neutral beam injector (NBI), the achievable plasma current and temperature will increase and a greater toroidal field will be necessary for the confinement of the plasma.

This work forms part of this project and will focus on the development of the magnetic diagnostics necessary for the plasma control and MHD unstable mode detection such as Rogowski and Mirnov coils. This diagnostic system must be precise and flexible enough to be used in all phases with minimum modifications.

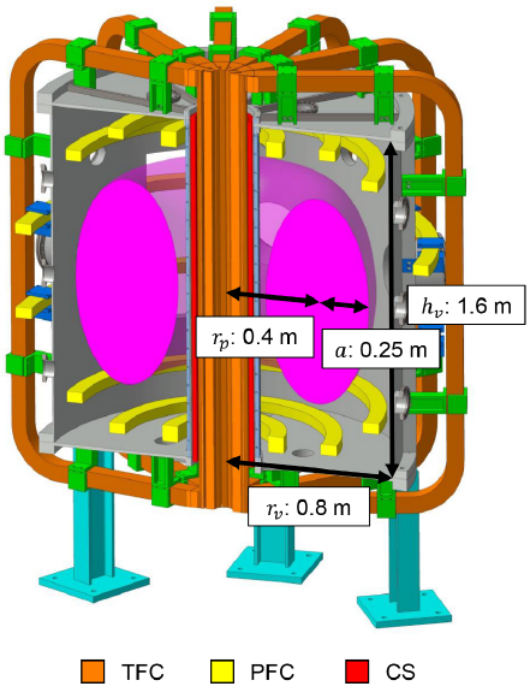

Figure 3.2: Schematic drawing of the geometry of SMART [14].

3.2 Rogowski coils.

Eight Rogowski coils are designed to be installed in SMART. One internal Rogowski coil mounted in the interior the vacuum chamber (VC) walls, one external Rogowski coil mounted on the exterior of the VC passing through the central stack and the CS and six smaller Rogowski coils mounted on the metallic casing of the PFC inside the VC (Fig. 3.3). With this configuration we aim to measure the plasma current, the current in the PFC and the Eddy currents in all conducting surfaces inside the VC.

Subtracting the PFC Rogowski coils' signal from the inner Rogowski coil's signal with the proper weights, will give us a direct measurement of the plasma current. Similarly, subtracting the inner Rogowski coil's signal from the outer Rogowski coil's will give us a direct measurement of the Eddy currents in the walls of the VC.

Unfortunately, due to space restrictions inside the center stack, the space in the center of the tokamak where the CS and TFC are located, the outer coil has to pass through the

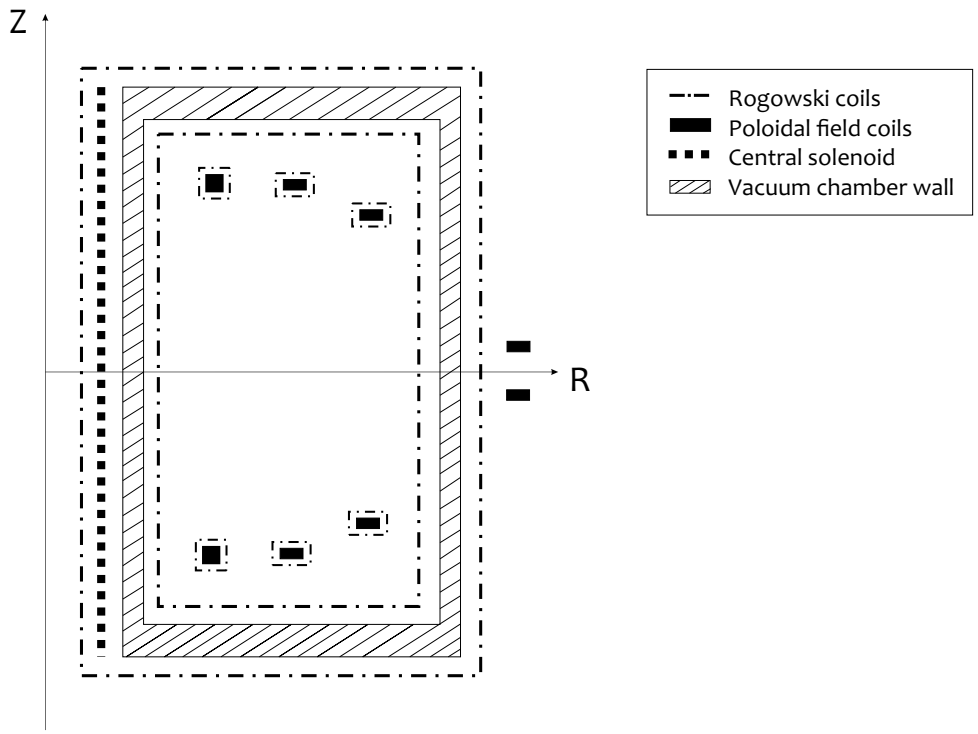

Figure 3.3: Schematic drawing of the positions of the Rogowski coils in SMART.

center of the CS picking up the current of 230 turns of wire. On top of that, this current is very out of center. With all this said, the current in the CS is known, so with some proper calibration, the signal created by the CS current should be correctable, but even then the precision of the measurements will suffer.

The inner and outer Rogowski coils will be constructed from KAPTON insulated copper wire wound around a non-magnetic conductive tube. This design will simplify greatly the compensation of the toroidal magnetic flux, as the conductive tube can be used as the return wire producing an almost perfectly centered compensation [17]. The parameters of these coils are described in Table 3.2.

Special care will have to be taken to avoid all the possible friction between the wires and the conductive tube due to vibrations during plasma shots, which could damage the wire insulation leading to short-circuits between the wire and the tube. To do so is recommended that the wire is wound at a slow pace and with constant tension and that the

	Inner Rogowski coil	**Outer Rogowski coil**
Wire diameter (mm)	0.6	0.6
Coil diameter (mm)	10	5
Coil length (m)	4.40	4.80
Number of turns	7333	8000
Self-inductance (mH)	1.355	0.4127
Resistance (Ω)	14.51	8.363
Resonance frequency (Hz)	250	452
Proportionality factor (10^{-6}Vs/kA)	184.8	51.58
Maximum estimated tension (V)	3.162	7.473

Table 3.2: Parameters for the inner and outer Rogowski coils. Resonance frequency estimated for a parasite capacitance of $300\mu F$.

wire is not bent at any sharp corners [18, 19].

Plasma configurations have been simulated with the FIESTA code [20] and the current profiles for the plasma, coils and Eddy currents have been obtained [16]. This simulations have been used to simulate the coils signal in a plasma shot for the last development phase (Fig. 3.4 and Fig 3.5).

Using these simulations and similar simulations where the currents were scaled down to represent the earlier phases, the necessary sensitivity of the coil was chosen so as to be able to measure the earlier phases with enough precision and signal to noise ratio while not saturating the digitalizer in the later ones.

The PFC are placed inside of a metal casing to protect them from the plasma. The objective of the six smaller Rogowski coils installed one on each of the PFC inside of the VC will be to measure the current in the PFC and the Eddy currents induced in the metal casings. The two PFC closer the the center are slightly bigger than the rest, so the Rogowski coils installed around those coils will be slightly longer. The parameters of the PFC Rogowski coils are described in Table 3.3.

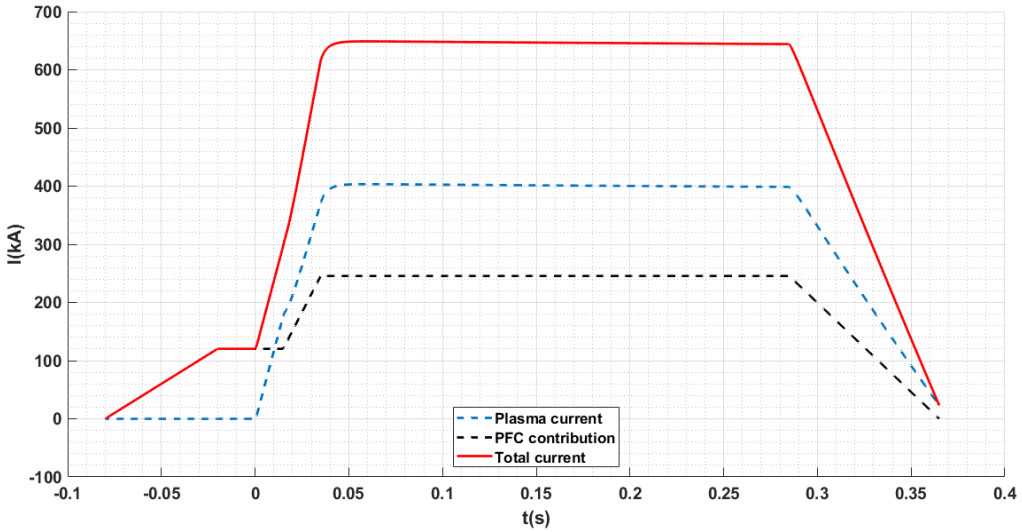

(a) Simulated currents measured by the inner Rogowski coil.

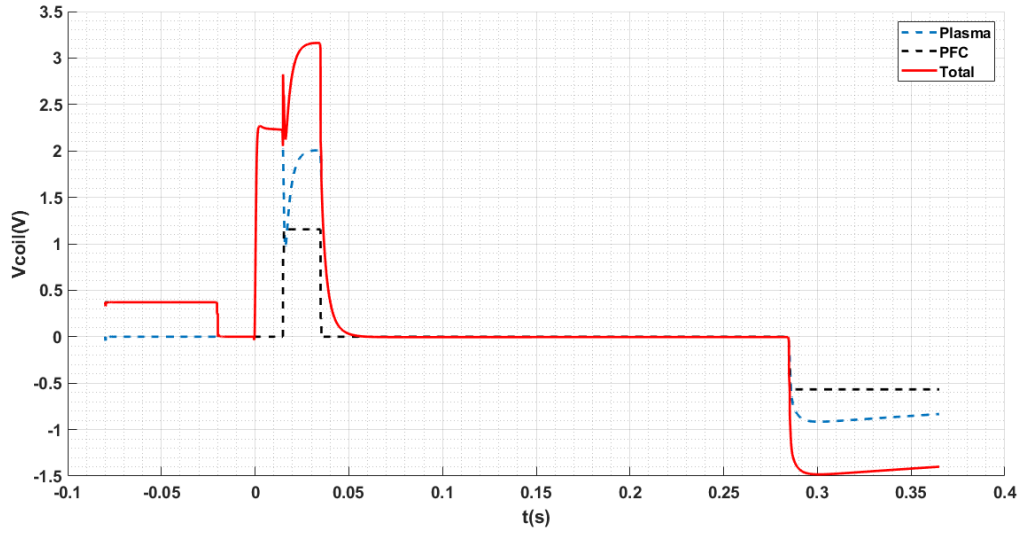

(b) Simulated signal from the inner Rogowski coil.

Figure 3.4: Simulations of the currents made with the FIESTA code and the Rogowski coil signal for the Rogowski coil installed inside of the VC.

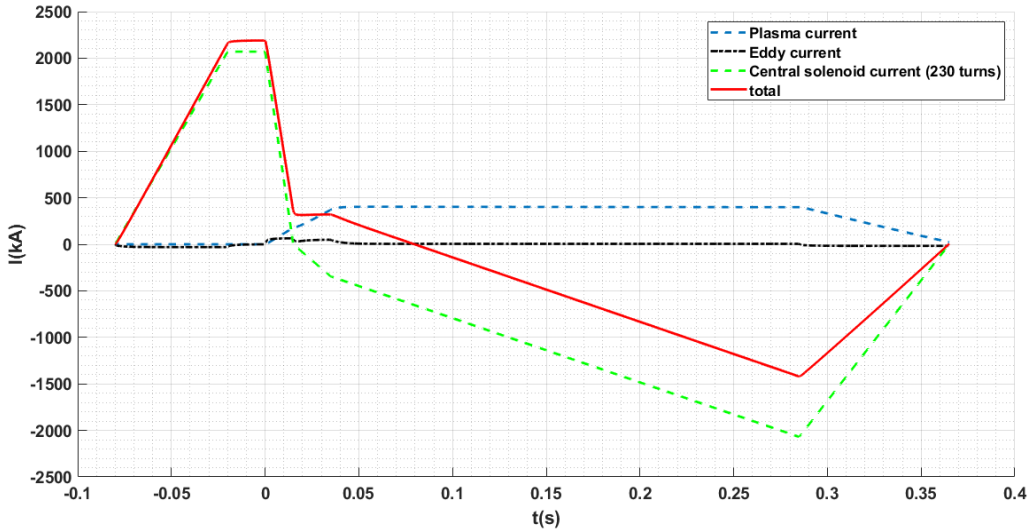

(a) Simulated currents measured by the outer Rogowski coil.

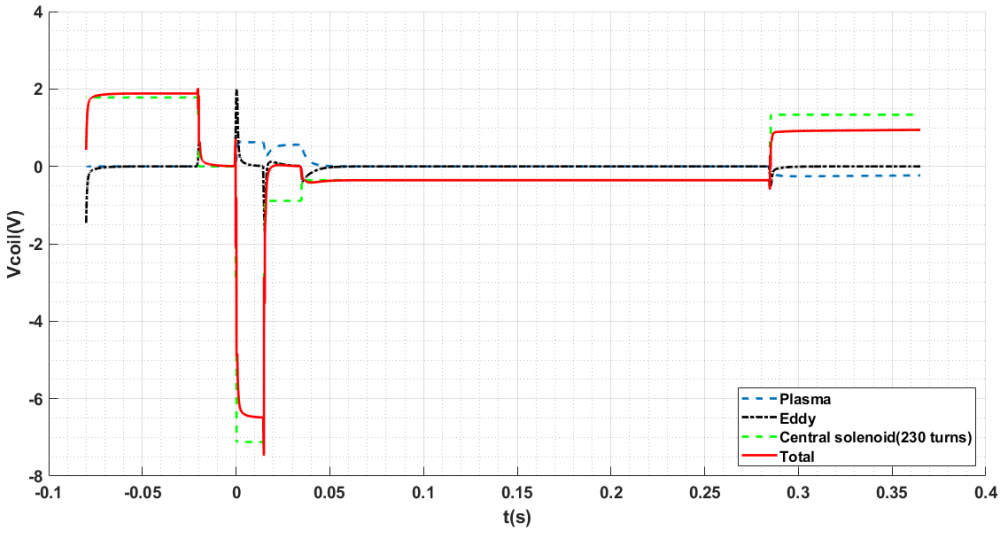

(b) Simulated signal from the outer Rogowski coil.

Figure 3.5: Simulations of the currents made with the FIESTA code and the Rogowski coil signal for the Rogowski coil installed outside of the VC.

	Short Rogowski coils	Long Rogowski coils
Wire diameter (mm)	0.4	0.4
Coil diameter (mm)	10	10
Coil length (cm)	32	40
Self-inductance (mH)	0.253	0.267
Resistance (Ω)	3.49	4.37
Resonance frequency (Hz)	629	562
Proportionaly factor (10^{-6}Vs/kA)	266.9	266.9
Maximum estimated tension (V)	0.210	0.210

Table 3.3: Parameters for the Rogowski coils installed in the PFC. The long Rogowski coils will be installed in the PFC closer to the center. Resonance frequency estimated for a parasite capacitance of $300\mu F$.

3.2.1 Rogowski signal integration.

Information about the plasma current and the Eddy currents are essential for the real-time control system as they hold critical information about the formation of MHD instabilities. Therefore we need the Rogowski coils signals to be integrated on real time so that we have access to that information. An analogical integrator will be used as it will greatly increase the speed of the calculations compared to doing them digitally.

A passive analogical integrator is just an RC circuit where the capacitor integrates the current that crosses the resistance. This basic design for a integrator circuit is functional but has two mayor disadvantages. Firstly, it's amplification is directly tied to it's cutoff frequency, f_c

$$V_o = \frac{1}{RC}\int V_i dt \tag{3.1}$$

$$f_c = \frac{1}{2\pi RC} \tag{3.2}$$

Secondly, to maximise the gain and bandwidth we need to reduce the input impedance which is not ideal as it would affect the tension in the coil.

The active integrator solves both of these problems. In an active integrator we use an operational amplifier (OPAMP) which has a high input impedance and lets us choose the gain of the circuit. In Fig 3.6 we can see the schematics of the circuit. The Rogowski coil is loaded with a resistor of a specific resistance, R_L, so as to critically dampen the RLC

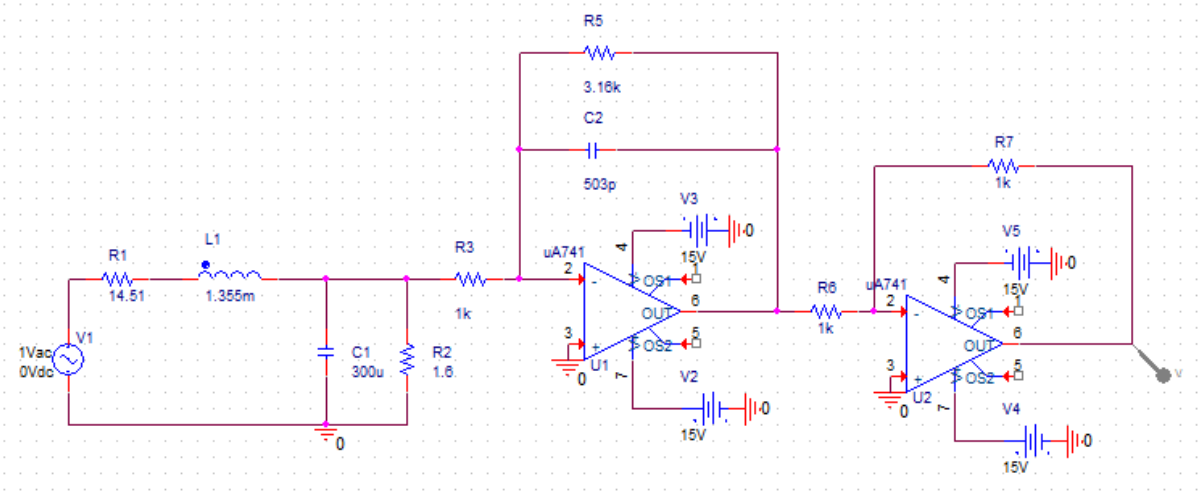

Figure 3.6: Circuit representation of the inner Rogowski coil with a load resistance conected to an active integrator.

circuit that represents the Rogowski coil to obtain the maximum bandwidth possible [8]. In this case we have a bandwidth of around 1kHz as we can see in the Bode diagram of the circuit (Fig. 3.7).

$$R_L = \frac{1}{2}\sqrt{\frac{L}{C}} \tag{3.3}$$

The capacitor in the integration circuit will get charged in the process of integration on each plasma shot, and must be discharged in between shots in order to properly process the signal from the next shot. To do so, a switch connected to a load resistance will be connected in parallel to the capacitor and it will be triggered in between shots.

3.2.2 Rogowski coil calibration proposal.

In order to characterize the Rogowski coils we need to determine their sensitivity and their frequency response. To determine the bandwidth of the coils, their self inductance and their parasitic impedance we propose the method used by the authors of [8].

The resonance frequency can be measured with a high frequency signal generator and an oscilloscope. If we excite the coils with a monochromatic signal while measuring the output with the oscilloscope and we start increasing the frequency, the signal should increase until we reach the resonance frequency, at which point the output signal will begging to drop.

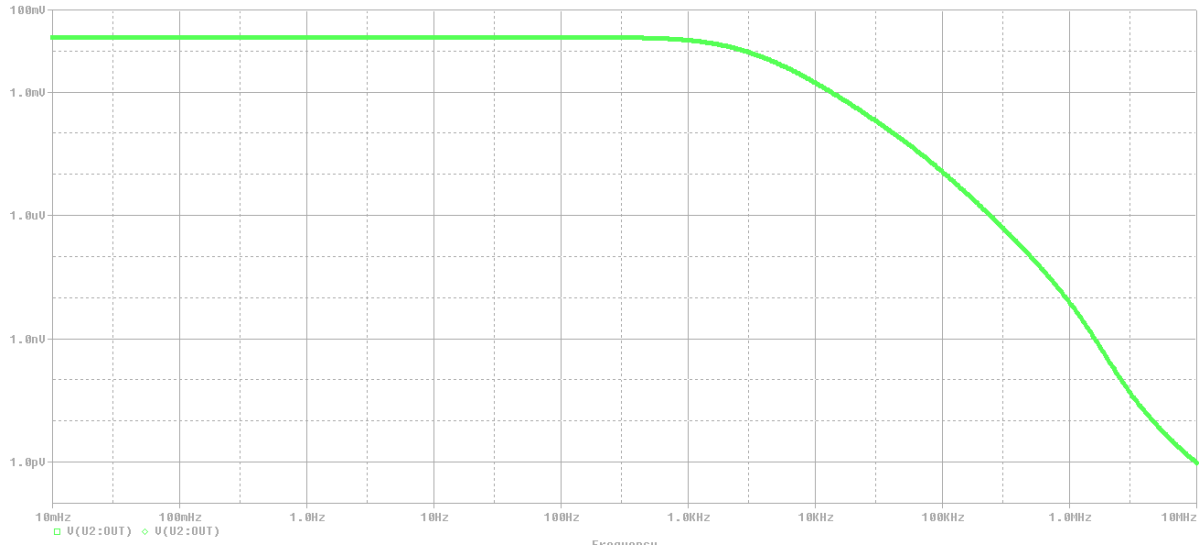

Figure 3.7: Simulated Bode diagram of the Rogowski-integrator circuit for the inner Rogowski coil.

We can then connect capacitors of capacitance, C_c in parallel lo the coil and repeat the process to measure the new resonance frequency. The parasitic capacitance of the coil and the self inductance can then be obtain by [8]

$$\begin{aligned} f_1 &= \frac{1}{2\pi\sqrt{LC}} \\ f_2 &= \frac{1}{2\pi\sqrt{L(C+C_c)}} \\ \frac{f_1}{f_2} = \sqrt{\frac{C+C_c}{C}} \quad &\rightarrow \quad C = \frac{C_c}{(f_1/f_2)^2 - 1} \\ L &= \frac{1}{(2\pi f_1)^2 C} \end{aligned} \tag{3.4}$$

Where f_1 is the resonance frequency without a capacitor and f_2 the resonance frequency with the capacitor. To increase the precision of this measurement we can repeat the process using multiple capacitors of different capacitance and doing a lineal regression to obtain C.

To determine the coils sensibilities, we propose using the already installed PFC and the CS to produce different current ramps, that can be measured by an industrial Rogowski coil, and recording the coils signals. Then, the coils sensitivities can be obtained by a linear regression. Keeping in mind that the Rogowski coil response is lineal for any current,

smaller currents can be used as long as the resulting signal has a good enough signal to noise ratio.

3.3 Mirnov coils.

Two sets of Mirnov coils have been designed for SMART, one will be used for the equilibrium reconstruction and the other will be used for the detection of high frequency instabilities. They will be fabricated using KAPTON insulated copper wire wound around a Teflon cylinder.

The need for two independent sets of coils arises from the great difference between the frequencies of change of the equilibrium fields ($\sim$ 100Hz) and the fields produced by instabilities ($\sim$ 10kHz-1MHz) [12]. As we have discussed, given the space constrains inside of the VC, it is practically impossible to build a coil with enough bandwidth to be able to measure the high frequency instabilities while having enough sensitivity to measure the equilibrium fields.

The set of Mirnov coils used for equilibrium reconstruction will consist of an array of 61 probes attached to the walls of the VC, 21 of them will be placed uniformly spaced in the poloidal direction and 41 uniformly in the toroidal direction, with one coil in the intersection of both arrays. This will allow us tho discern a total of $M = 20$ toroidal modes and $N = 10$ poloidal modes.

The equilibrium Mirnov coils will be used for the real time equilibrium reconstruction. As real time control will not need to resolve that many modes, each array will be divided into two so as to provide duplicity, each coil will have it's symmetrical coil as backup in case any of the coils fail during a shot.

Each equilibrium Mirnov coil will consist of three small multi-layer coils ($\sim 1cm \times 1cm \times 1cm$) oriented in orthogonal directions, so as to measure all the components of the magnetic field on each position. They have been designed to be very compact in order to fit in the tight space between the central VC wall and the plasma.

The unintegrated signal of the equilibrium Mirnov coils will also allow us to detect low frequency instabilities of up to $\sim$ 1kHz, at which point the signal will stop to increase

with frequency and the signal due to the instability will become small compared to the signal created by the equilibrium fields.

Six Mirnov coils placed at different positions in the toroidal direction will be used for the detection of high frequency instabilities. They have been designed so as to maximise the bandwidth, by reducing the self inductance and parasitic capacitance of the coils. To do so, the number of turns per unit length has been greatly reduced by increasing the spacing between turns and by only using one layer of winding.

The objective of the design was to reach the 1MHz of bandwidth needed to measure high frequency Alfvén modes in the plasma. The final bandwidth of the coils will depend on the parasitic capacitance of the coils, which will change depending on the final construction of the coils.

To reduce this capacitance special care will have to be taken so the winding is uniform and the output cables are as short as possible [12]. With the chosen design, 1MHz bandwidth can be achieved if the parasitic capacitance is kept bellow $0.1\mu F$.

Once the signal is transported outside of the VC the signal will be transported using a properly adapted transmission line, in this case a coaxial cable, to preserve the integrity of the high frequency components of the signal.

The parameters of both the equilibrium and instability detection Mirnov coils are described in Table 3.4. The ration between the coils length and radius has been chosen to be $R/l = 0.866$ to minimize the effects of the inhomogeneous field inside of the coils [21].

3.3.1 Mirnov coil calibration proposal.

The sensitivity of the Mirnov coils is directly determined by their effective area, but geometrical measurements are not the most precise method for the determination of the effective area. Our calibration proposal is to use a solenoid or a set of Helmholtz coils excited with a monochromatic sinusoidal signal to create magnetic fields of different amplitude and frequency. The effective area can be obtained from a linear regression of the coil signal against the created field.

	Equilibrium Mirnov coils	**Instability Mirnov coil**
Wire diameter (mm)	0.25	0.6
Core diameter (mm)	2.2	40
Coil length (cm)	9	46
Number of turns	360	5
Number of layers	10	1
Self-inductance (μH)	375	0.881
Resistance (Ω)	1.91	0.038
Resonance frequency (kHz)	0.821	169
Effective area (cm^2)	74.75	64.73

Table 3.4: Parameters of the designed Mirnov coils. The instability detection Mirnov is wound with 8mm of spacing in between turns. Resonance frequencies calculated for a parasitic capacitance of $100\mu F$ for the equilibrium coils and a conservative $1\mu F$ for the instability coils.

The parasitic capacitance can be determined with a similar method as the one described in the Rogowski coil calibration section for the same objective. The resonance frequency can be obtained connecting the coil to a high frequency signal generator and increasing the frequency until the resonance frequency is reached, at which point the tension on the coil will start to fall.

3.4 Poloidal flux loops and diamagnetic loops.

Twelve poloidal flux loops will be installed inside of the VC, one attached to the metallic casing of each PFC, three attached to the exterior wall of the VC and three attached to the interior wall. Each poloidal flux loop will be built from a single turn of KAPTON insulated copper cable doing a full rotation in the toroidal direction.

The poloidal flux loops will be connected deferentially to one of the flux loops inside of the central horizontal plane that will be used as reference to cancel the magnetic flux created by the CS. Their integrated signal will be proportional to the magnetic flux in the magnetic surface that contains them.

Multiple loops will be used to determine the one-turn voltage of the plasma, which will be equal to the unintegrated signal of the coils once the contribution of the CS is removed. The one-turn voltage will then be used to determine the conductivity of the plasma.

Six diamagnetic loops will be installed outside of the VC, each on in the mid-plane between two of the twelve TFC, in an alternating pattern. Each diamagnetic loop will be built from a single turn of KAPTON insulated copper wire doing a full rotation in the toroidal direction and passing through the center stack of the tokamak.

As we have discussed, the main contributor to the signal created in the diamagnetic loops will be the toroidal magnetic flux created by the TFC. To obtain the component of the signal corresponding to the diamagnetism of the plasma, the diamagnetic loops will be calibrated in the absence of plasma. The weighted signals of Mirnov coils close to the loop and the Rogowski coil surrounding the power supply of the TFC will be subtracted from the signal of the loop to obtain a zero signal in absence of plasma.

When plasma is introduced inside of the tokamak, the calibrated signal will correspond to the reduction in toroidal flux caused by the diamagnetism of the plasma.

Chapter 4

Conclusions

In this work we have described some of the diagnostics that will compose the magnetic diagnostics system in a tokamak and we have designed some of the magnetic sensors that will be installed in the SMall Aspect Ratio Tokamak of the University of Seville.

The chosen design of the Rogowski coils, Mirnov coils, poloidal flux loops and diamagnetic loops has been described in detail, including their geometrical design and position, the chosen materials and derived electromagnetic parameters.

With these diagnostics we will be able to measure many properties of the plasma inside of the tokamak, including magnetic fields, the plasma current, Eddy currents in the vacuum chamber walls, the plasma shape and position, the plasma conductivity and self inductance and the plasma pressure.

These diagnostics will also play an important role in the real time control of the plasma and in the detection of instabilities inside of the plasma, helping to prevent disruptions during a plasma shot.

Finally, we would like to reiterate that the design of this components is in it's conceptual phase, and may be subject to some revisions before the final diagnostic system is completely installed.

Nevertheless, this work will be expanded on in other publications to include any possible changes and the final results of the construction and calibration of the diagnostics.

Bibliography

[1] Rubens A. Dias, Cristiano R. Mattos, and José A. P. Balestieri. The limits of human development and the use of energy and natural resources. *Energy Policy*, 34(9):1026–1031, 2006.

[2] Mitsuru Kikuchi and Karl Lackner. *Fusion Physics*. IAEA, 2012.

[3] John Wesson. *Tokamaks*. Oxford University Press, 01 2004.

[4] Francis Chen. *Introduction to Plasma Physics and Controlled Fusion*. Springer, 2016.

[5] I. H. Hutchinson. *Principles of Plasma Diagnostics*. Cambridge University Press, 2005.

[6] E. J. Strait. Magnetic diagnostic system of the diii-d tokamak. *Review of Scientific Instruments*, 77(2):023502, 2006.

[7] Slawomir Tumanski. Induction coil sensors—a review. *Measurement Science I& Technology - MEAS SCI TECHNOL*, 18, 03 2007.

[8] Muhammad Shafiq, Lauri Kutt, Matti Lehtonen, Tatu Nieminen, and Murtaza Hashmi. Parameters identification and modeling of high-frequency current transducer for partial discharge measurements. *IEEE Sensors Journal*, 13(3):1081–1091, 2013.

[9] Luka Ferkovic, Damir Ilic, and Roman Malaric. Mutual inductance of a precise rogowski coil in dependence of the position of primary conductor. *Instrumentation and Measurement, IEEE Transactions on*, 58:122 – 128, 02 2009.

[10] Branislav Djokić. The design and calibration of rogowski coils. *NCSLI Measure*, 4:62–75, 06 2009.

[11] K. J. Chung, Y. H. An, B. K. Jung, H. Y. Lee, C. Sung, Y. S. Na, T. S. Hahm, and Y. S. Hwang. Design features and commissioning of the versatile experiment spherical torus (VEST) at seoul national university. *Plasma Science and Technology*, 15(3):244–251, mar 2013.

[12] E. J. Strait, E. D. Fredrickson, J.-M. Moret, and M. Takechi. Chapter 2: Magnetic diagnostics. *Fusion Science and Technology*, 53(2):304–334, 2008.

[13] Y-K.M. Peng and D.J. Strickler. Features of spherical torus plasmas. *Nuclear Fusion*, 26(6):769–777, jun 1986.

[14] M. Agredano-Torres, J.L. Garcia-Sanchez, A. Mancini, S.J. Doyle, M. Garcia-Munoz, J. Ayllon-Guerola, M. Barragan-Villarejo, E. Viezzer, J. Segado-Fernandez, D. Lopez-Aires, J. Toledo-Garrido, P.F. Buxton, K.J. Chung, J. Garcia-Dominguez, L. Garcia-Franquelo, M.P. Gryaznevich, J. Hidalgo-Salaverri, Y.S. Hwang, J.I. Leon-Galvan, and J. Maza-Ortega. Coils and power supplies design for the smart tokamak. *Fusion Engineering and Design*, 168:112683, 2021.

[15] A. Mancini, J. Ayllon-Guerola, S.J. Doyle, M. Agredano-Torres, D. Lopez-Aires, J. Toledo-Garrido, E. Viezzer, M. Garcia-Muñoz, P.F. Buxton, K.J. Chung, J. Garcia-Dominguez, J. Garcia-Lopez, M.P. Gryaznevich, J. Hidalgo-Salaverri, Y.S. Hwang, and J. Segado-Fernández. Mechanical and electromagnetic design of the vacuum vessel of the smart tokamak. *Fusion Engineering and Design*, 171:112542, 2021.

[16] S.J. Doyle, D. Lopez-Aires, A. Mancini, M. Agredano-Torres, J.L. Garcia-Sanchez, J. Segado-Fernandez, J. Ayllon-Guerola, M. Garcia-Muñoz, E. Viezzer, C. Soria-Hoyo, J. Garcia-Lopez, G. Cunningham, P.F. Buxton, M.P. Gryaznevich, Y.S. Hwang, and K.J. Chung. Magnetic equilibrium design for the smart tokamak. *Fusion Engineering and Design*, 171:112706, 2021.

[17] J. Coonrod, M. G. Bell, R. J. Hawryluk, D. Mueller, and G. D. Tait. Magnetic diagnostics and feedback control on tftr (invited). *Review of Scientific Instruments*, 56(5):941–946, 1985.

[18] M. Baruzzo, G. Artaserse, R.B. Henriques, S. Gerasimov, N. Lam, P.J. Lomas, R. Otin, F. Rimini, M. Tsalas, and S. Van Boxel. Fault analysis and improved design of jet in-vessel mirnov coils. *Fusion Engineering and Design*, 150:110863, 2020.

[19] A.S. Bozek and E.J. Strait. Manufacturing of magnetic probe coils for diii-d. In *20th IEEE/NPSS Symposium onFusion Engineering, 2003.*, pages 336–339, 2003.

[20] L. Pangione, G. McArdle, and J. Storrs. New magnetic real time shape control for mast. *Fusion Engineering and Design*, 88(6):1087–1090, 2013. Proceedings of the 27th Symposium On Fusion Technology (SOFT-27); Liège, Belgium, September 24-28, 2012.

[21] H. Zijlstra. *Experimental methods in magnetism. By H. Zijlstra.* Series of monographs on selected topics in solid state physics ; 9. North-Holland Pub. Co., Amsterdam, 1967.